Sens. & Instrumen. Food Qual. (2008) 2:215–224
DOI 10.1007/s11694-008-9055-z

ORIGINAL PAPER

Differentiation of toxigenic fungi using hyperspectral imagery

Haibo Yao · Zuzana Hruska · Russell Kincaid · Robert L. Brown · Thomas E. Cleveland

Received: 13 December 2007 / Accepted: 21 May 2008 / Published online: 25 June 2008

Abstract Some pathogenic fungi, *Aspergillus flavus* for example, produce mycotoxins that can contaminate grain products including wheat and corn. The contaminated grain poses a threat to the health of both humans and animals. Therefore, from the perspective of food safety and protection, it is important to detect and identify the different toxin-producing fungi encountered in food production. Earlier studies examined various spectral-based, non-destructive methods for the detection of fungi and toxins. The present report focused on the feasibility of using spectral image data for fungal species classification. A tabletop hyperspectral imaging system, VNIR-100E, was used for spectral and spatial data acquisition. A total of five fungal species were selected for a two-part experiment: *Penicillium chrysogenum, Fusarium moniliforme (verticillioides), Aspergillus parasiticus, Trichoderma viride*, and *Aspergillus flavus*. All fungal isolates were cultured on media under laboratory conditions and were imaged on day 5 of growth. The objective of the study was to use visible near-infrared hyperspectral imagery to differentiate fungal species. Results indicate that all five fungi are highly separable with classification accuracy of 97.7%. In addition, all five fungi could be classified by using only three narrow bands (bandwidth = 2.43 nm) centered at 743 nm, 458 nm, and 541 nm.

Keywords Hyperspectral image · Fungi · Classification

H. Yao (✉) · Z. Hruska · R. Kincaid
Institute for Technology Development, Building 1103, Suite 118, Stennis Space Center, MS 39529, USA
e-mail: hyao@iftd.org

R. L. Brown · T. E. Cleveland
SRRC, ARS, USDA, 1100 Robert E. Lee Boulevard, New Orleans 70124, LA, USA

Introduction

Fungi grow almost everywhere and on most substances under humid conditions. Some fungi produce toxins and pose a threat to humans and animals. Certain fungi, *Aspergillus Flavus* (*A. flavus*) for instance, produce a toxic secondary metabolite called aflatoxin. Aflatoxin contaminated corn is toxic to domestic animals when ingested in feed and is associated with liver and lung cancer in human beings [1]. Consequently, aflatoxin levels in food and feed are regulated by the Food and Drug Administration (FDA) in the US. FDA requires less than 20 ppb of aflatoxin levels in feed and food for interstate commerce [2]. As a result, the ability to detect *A. flavus* and its toxic metabolite, aflatoxin (by HPLC or thin-layer chromatography [3]), is crucial to the grain industry, especially in corn production. In addition to corn, *A. flavus* is known to infect unprocessed cowpea and groundnut (e.g. peanuts) during storage, along with certain *Trichoderma* and *Penicillium* species [4]. Fumonisins are a family of mycotoxins produced by certain *Fusarium* species, another mold that is connected to food and feed production [5]. These molds infect rice as well as other cereal grains including corn [5, 6]. Fumonisins affect cellular metabolism in plants and animals and are acutely toxic to horses and swine [5]. Additionally, fumonisins have been found to have carcinogenic properties in rats [5] and are associated with human esophageal cancer [7].

Accordingly, it is important to detect and identify different toxin-producing fungi. An important benefit derived from fungal identification procedures is knowing which toxin may be present in a given sample. Once a fungus is identified, it is possible to extrapolate the specific toxin or toxins that may be present as a consequence. For example, the presence of *Aspergillus flavus* does not necessarily

indicate harmful levels of aflatoxin. However, it does mean that the potential for aflatoxin production is present. Another example is that some fungi such as *Aspergillus niger* and *Trichoderma viride* can inhibit the growth of *A. flavus* and subsequent aflatoxin detection [8]. Thus, correct identification of a fungus can be helpful in detecting the presence of specific toxins associated with the identified organism. Fungal detection/identification systems may be applied as tools in food inspection, homeland security, household inspection, mold remediation, and environmental protection among others.

Some studies explored the use of aflatoxin fluorescence response for qualitative identification of aflatoxin-producing fungi [9, 10]. New methods developed in recent years include DNA-based analytical methods (e.g. Polymerase Chain Reaction—PCR) for fungal detection [11], and enzyme-linked immunoassays for mycotoxin detection [12]. Morphologic information during *A. flavus* growth also can be used for the determination of aflatoxin production [13]. The toxin detection was based on direct visualization of a beige ring surrounding *A. flavus* colonies after an incubation time of 3 days at 28 °C plated on a yeast extract sucrose medium (YES), supplemented with a specific cyclodextrin and sodium desoxycholate. The additive, cyclodextrin, can enhance the natural fluorescence of aflatoxin [14].

Other research carried out for the development of rapid, non-invasive ways for fungal identification includes a study by Birth and Johnson [15], based on optical measurements using fluorescence data for fungal detection on corn. The study found that the ratio between two measurements of the fluoresced energy (at 442 and 607 nm) gave the most consistent results. One study [16] suggested using UV photography for screening of fungi. In this approach, a UV light source centered at 365 nm wavelength was used to irradiate samples of different strains of *Aspergillus*. Images were taken using a UV lens with a Nikon F3 camera. The results showed that aflatoxin-producing fungi such as *A. flavus* and *A. parasiticus* aggregated in gray or black colonies, while the non-aflatoxin producing taxa such as *A. oryzae* appeared as white colonies. Further study [17] pointed out that the naturally occurring *A. flavus* population might include a majority of strains that are non-toxigenic but exhibit BGYF (bright greenish yellow fluorescence) and are thus aflatoxin "false-positives" when examined with an ultraviolet light at 365 nm. Colony morphology and color microscopy, as well as biochemical tests were employed for fungal group identification [18]. Fourier Transform Infrared (FTIR) spectroscopy was also utilized for *A. flavus* detection on corn [19–22]. The FTIR studies examined differences in spectral features of fungi and different corn backgrounds. Although the process was non-destructive, the instrumentation involved can be costly and the sample size somewhat limited [23].

An imaging spectrometer or hyperspectral imager can produce hyperspectral images with spectral and spatial resolution. A single hyperspectral image has a spectral resolution between one and several nanometers, with the number of bands ranging from tens to hundreds. The neighboring image bands are highly correlated and data reduction is generally needed before classification of a hyperspectral image. High spectral resolution images can be used to study either the physical characteristics of an object at each pixel by looking at the shape of the spectral reflectance curves or the spectral/spatial relationships of different classes using pattern recognition and image processing methods.

Traditionally, hyperspectral imagery was employed in earth remote sensing applications using aerial or satellite image data. Most recently, low cost portable hyperspectral sensing systems became available for laboratory-based research. The literature reports several agricultural studies where hyperspectral technology was applied for detection of fungal contamination [24] and bruising [25] in apples, fecal contamination [26, 27] and skin tumors [28] on chicken carcasses, as well as prediction of oil and oleic acid concentrations in individual corn kernels [29] and corn genotype identification [30].

The objective of the current research was to develop a relatively simple, non-invasive method to rapidly identify fungi by means of hyperspectral images. The study used visible-near-infrared hyperspectral images taken by a push-broom hyperspectral sensor to identify different toxin and non-toxin producing fungal isolates. It was assumed that the specific spectral signatures associated with each fungus would provide enough information for discriminating between different fungi, including different species within a single genus.

Materials and methods

Instrumentation

The VNIR 100E hyperspectral imaging system (Institute for Technology Development (ITD), Stennis Space Center, MS 39529) was utilized for image acquisition in the study (Fig. 1). The VNIR 100E incorporates a patented line scanning technique [31] that requires no relative movement between the target and the sensor. By scanning an input image within the focal plane of a front lens and dispersing an input image line vertically as a function of the spectral wavelengths, the hyperspectral focal plane scanner eliminates the requirement of a mobile platform in a pushbroom scanning system. The sensor uses a prism-grating prism to separate incoming light into component wavelengths. Image data are recorded by a 12-bit CCD camera with a 1,376 × 1,040 pixel array. The variable binning capability

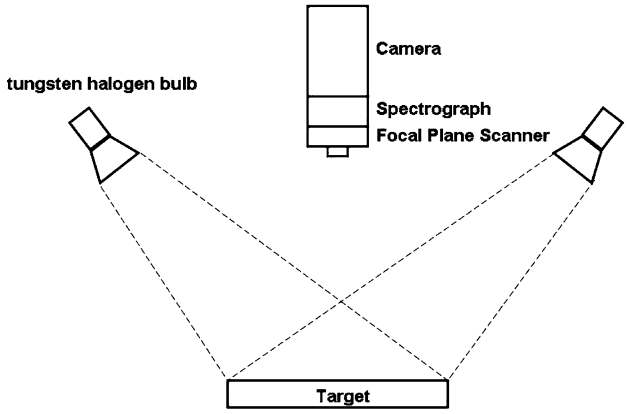

Fig. 1 Schematic overview of the imaging system using the VNIR-100E hyperspectral imaging sensor

of the camera allows image acquisition at user specified spatial and spectral resolutions. Each output image contains a complete reflectance spectrum from 400 to 1,000 nanometers. In order to illuminate the target area, two MR16 tungsten halogen bulbs with dichroic reflectors are mounted with the sensor on an adjustable camera stand. The lamps are fitted with diffusion and color-balancing filters in order to resolve specular reflectance and to simulate natural lighting.

ITD has also developed a software application (HyperVisual®) for use with the VNIR 100E sensor. The software is designed to perform image capture as well as various pre-processing functions. Within the HyperVisual® software application, the image capture parameters for the vertical and horizontal binning are user defined. The horizontal binning determines the across-track width of the image, while the vertical binning determines the number of spectral bands. For this experiment, spatial binning was set at 2 for a resolution of 688 pixels in image width. Spectral binning was set to 4 to return 260 spectral bands. Exposure time was set at 145 ms to maximize the range of the recorded data values without exceeding 4,096 digital counts for the 12 bit system. Based on the above parameters, the proper speed required to move the lens in order to obtain true geometry in the image was calculated as 0.086 mm/s. Memory specific maximums of 525 lines were captured at these settings. The sensor was focused with a 35 mm lens and set at a distance of 46.36 cm from the surface of the fungal plate to the camera lens. The resulting footprint was approximately 11.8 × 9.2 cm [8] in area, thus approximate pixel resolution of the system was 0.175 × 0.175 mm [8]. The spectral resolution was 2.43 nm.

Experiment design and procedure

Five different fungi, *Penicillium chrysogenum, Fusarium moniliforme (verticillioides), Aspergillus parasiticus, Trichoderma viride, and Aspergillus flavus*, were used in the present study. The fungi were selected because of their known involvement in food infection. The toxigenic properties of each fungus are listed in Table 1. Among the five fungi listed, four were from different genera. Two fungi were selected from the same genus (*Aspergillus*) but different species in order to test the sensitivity of the imaging system. All the fungi were obtained from the Food and Feed Safety laboratory, Southern Regional Research Center (SRRC), United States Department of Agriculture (USDA), New Orleans, Louisiana. Subsequent fungal culture preparation and imaging was also conducted at the SRRC research Laboratory.

The experiment had two parts, A and B. Fungi were cultured on plastic Petri-dishes/plates on potato dextrose agar (PDA) in an incubator at 30 °C. In Part A, each fungus was inoculated at the center of a single plate with 10 μL of the respective fungal inoculum. Each isolate had two replications resulting in a total of ten plates. In Part B, all five isolates were inoculated at different spots on the same plate with 5 μL of inoculum (see Fig. 2 for inoculation locations of fungi). The identical inoculation sequence was repeated on five different plates, resulting in five replicates.

Image acquisition

Images for both experiments were taken on the 5th growth day using experiment settings described previously. The 5th growth day produced optimum images of all five fungi. All

Table 1 Toxigenic fungi used in the experiment

Item	Name of fungus	Toxin producing	Name of toxin
1	*Fusarium verticillioides*	Yes	Fumonisin
2	*Aspergillus flavus*	Yes	Aflatoxin
3	*Trichoderma viride*	Yes	Trichodermin, Trichotoxin A
4	*Aspergillus parasiticus*	Yes	Aflatoxin
5	*Penicillium chrysogenum*	Yes	Roquefortine C

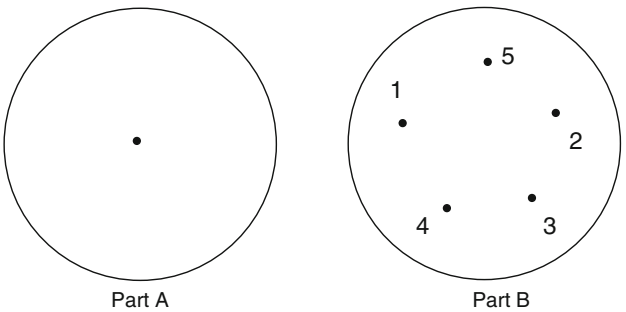

Fig. 2 Fungal inoculation schema for both parts of the experiment. The black dots are the designated inoculation spots within the Petri-plate. The numbers in Part B represent the item numbers of different isolates. See Table 1 for the name of each isolate

dishes from each experiment were imaged in random order. For image calibration, a dark current image and a standard reflectance image were taken in each experiment before imaging the fungi. The dark image data were taken with the camera lens completely blocked and a white diffuse reflectance standard panel 25.4 × 25.4 cm^2 (Spectralon: SRT-99-100 UV-VIS-NIR Diffuse Reflectance Target, LabSphere Inc.) was used to take the reference reflectance data.

Hyperspectral image preprocess

A series of pre-processing steps were applied to each raw hyperspectral image in order to set up the correct image orientation, minimize the image noise, and calibrate light reflectance. The following preprocessing steps were programmed in HyperVisual® and executed in batch mode: (1) Geometric correction; (2) Data format conversion; (3) Wavelength assignment; (4) Scene calibration to percentage reflectance; (5) Noisy band removal; (6) Random noise removal.

The geometric correction step rotates the plate image 180° to the correct orientation. The data format conversion step converts image data from two-byte integer to four-byte floating point. The wavelength assignment step sets each band with its appropriate wavelength. The imaging sensor recorded only raw digital counts of reflectance, therefore, a dark and a reference scan were needed to convert the raw digital counts to percent reflectance. For reflectance calibration, the following equation was used:

$$Reflectance_\lambda = \frac{S_\lambda - D_\lambda}{R_\lambda - D_\lambda} \times 100\% \quad (1)$$

where $Reflectance_\lambda$ is the reflectance at wavelength λ; S_λ is the sample intensity at wavelength λ; D_λ is the dark intensity at wavelength λ; R_λ is the reference intensity at wavelength λ.

Because image data from 400 nm to 450 nm and from 900 nm to 1,000 nm contains relatively high levels of background noise, image bands within the above spectral regions were cut during the noisy band removal step. After the above pre-processing steps, spectral curves for individual pixels still showed random noise. The random noise removal step ran a low pass spectral filter. The low pass filter had a window size of five and ran a moving average along the wavelength for each pixel. After preprocessing, the calibrated image had 185 bands with wavelength range from 450 nm to 900 nm. The resulting image of 688 × 525 pixels had an image size of 267 Mbytes.

Image processing and data analysis

Part A of the experiment was intended for fungal classification and pure fungal signature extraction. Each fungal isolate was plated in duplicate. The two replications of all five fungi were merged together to form one large image. Next, a small area of growth for each fungus was selected as a training region of interest. The selection focused on a region of older 'mature' growth of the fungal culture. Similarly, validating data was also selected from the mosaic image.

Different supervised classification algorithms were first tested in order to determine which image classification was best suited for our data. The algorithms tested were, parallel piped, Spectral Angle Mapper, minimum distance, Mahalanobis Distance, Maximum Likelihood (ML), and binary encoding, available in a software package, ENVI [32]. Based on preliminary results, the Maximum Likelihood algorithm was deemed best for further investigation. One drawback of the chosen algorithm was data processing time depending on different data formats. ENVI can support both Band Sequential (BSQ) data and Band Interleave (BIL) data. It took approximately 44 min with the BSQ data format, or 14 min with the BIL data format to complete the 3 G byte, 185 bands mosaic image on a 2.4 G hertz Pentium computer with 3.5 G bytes of memory.

At this point, image dimension reduction was needed to speed up the classification process. A previous study [33] indicated that classification accuracy for high dimension data such as hyperspectral image could be improved by reducing dimensionality or by increasing the number of training samples. Since the initial ML classification with all 185 bands took a long time to process, a reduced image space was desired in order to reduce the amount of time for image classification. In addition, because neighboring hyperspectral images are highly correlated with each other, this correlation affects correct estimation of class statistics for a parametrical classifier such as ML, which may lead to decreased classification accuracy. Thus, a reduced image space also helps improve class statistics estimation, and consequently improves the overall classification accuracy. In this paper the training data was extracted and processed in a SAS STEPDISC [34] procedure using the forward selection option to obtain the most significant image bands. Forward band selection starts with no bands in the model. At each step, PROC STEPDISC enters the band that contributes most to the discriminatory power of the model as measured by Wilks' Lambda, the likelihood ratio criterion. When none of the unselected bands meet the entry criterion, the forward selection process stops. Based on the results from the STEPDISC procedure, the top 10 image bands were used in the ML classification. The classification time was dramatically reduced to less than 1 minute for both the BSQ and BIL formats. Classification accuracy was subsequently assessed at this point.

Once the classified image was obtained, the classified region for each fungus was used to extract a pure fungal signature and to compute class statistics such as mean and covariance. This information can be assumed as standard

Table 2 Selected validation pixels for experiment part B. The training data was obtained from experiment part A

Fungal class	Pixel number				
	Fusarium	*A. flavus*	*Trichoderma*	*A. parasiticus*	*Penicillium*
Validation	54,835 (17.19%)	72,868 (22.84%)	95,888 (30.06%)	65,387 (20.50%)	30,047 (9.42%)

Table 3 Selected training and validation pixels for experiment part A

Fungal class	Pixel number				
	Fusarium	*A. flavus*	*Trichoderma*	*A. parasiticus*	*Penicillium*
Training	7,248 (19.85%)	7,135 (19.54%)	7,597 (20.81%)	7,858 (21.52%)	6,674 (18.28%)
Validation	79,282 (17.90%)	91,130 (20.57%)	198,231 (44.75%)	63,322 (14.30%)	10,999 (2.48%)

classification training data and used for future classification and identification.

In part B of the experiment, multiple fungi were classified based on training data (pure fungal signatures) obtained from experiment part A (Table 2). Similar to experiment part A, the five replicate images, each with five cultured fungi in one dish, were mosaiced into a single image. The validation pixel number for each isolate is showed in Table 3. ML classification was run with the 10 most significant image bands identified in experiment part A. Classification accuracy was assessed by using a separate data set.

Results and discussion

Experiment part A

Figure 3a depicts the true color image for all fungal isolates in experiment part A. Different isolates exhibit different growth patterns. For example, *Penicillium* grew over only a small fraction of the Petri dish, indicating slow growth over the 5-day culturing period. On the other hand, *Trichoderma* displayed rapid growth as it expanded over the entire Petri dish. The other three fungi, *Fusarium*, *A. flavus*, and *A. parasiticus* showed moderate growth. On PDA medium, *Fusarium* has a distinct white (with pink/lavender in the center) color compared to the other fungi. The two *Aspergilli* have similar growth patterns and slightly different color.

As previously stated, when performing image classification the initial ML classification with all 185 bands took a long time to process. A reduced image space was desired in order to reduce the amount of time for image classification. Also, because neighboring hyperspectral images are highly correlated, the correlation affects correct estimation of class statistics for the parametrical classifier ML, which in turn leads to decreased classification accuracy. Therefore, reducing image space, by the stepwise discriminant analysis ranking of image bands used in the present paper, helped improve the class statistics estimation, and consequently improved the overall classification accuracy. Table 4 presents the first 10 image bands selected from stepwise discriminant analysis. Within the 10 bands, three are in the blue region (450 nm, 458 nm, and 478 nm), three are in the green region (509 nm, 541 nm, 572 nm), two are in the red region (616 nm, 670 nm), and two are in the near infrared region (743 nm, 864 nm). All bands are statistically significant with $P < 0.0001$. The partial R-square (the squared partial correlation) is listed from most to least, ranging from 0.97 to 0.16. The Wilks' Lambda ranged from 0.025 to 6.81E-05. In this study, Wilks' lambda is the likelihood ratio statistic for testing the hypothesis that the means of the fungal classes based on the selected image bands are equal in the population. Generally, lambda is close to zero if any two groups are well separated. Average Squared Canonical Correlation (ASCC) describes how all the fungal classes are separated. ASCC is close to 1 if all classes are well separated and if all or most directions in the discriminant space show good separation for at least two fungal classes.

Figure 3b indicates regions of interest (ROIs) of both training and validation pixels. Figure 4 demonstrates the ML classification results for part A of the experiment. The results show that all the 'mature' fungi were classified relatively correctly. The new growth regions of some fungi, i.e., the ring shape regions of *Fusarium*, *A. parasiticus*, and *A. flavus*, were mistakenly assigned to other classes. The possible reasons for this discrepancy are: (1) the training classes were defined using the mature fungal growth regions; (2) the new growth regions for some fungi were spreading fast and thus were sparsely covering medium (background), resulting in a spectral signature that was a mixture of fungus and agar. On the other hand, *Penicillium* and *Trichoderma* had much less misclassification from the new growth area of the fungal colonies.

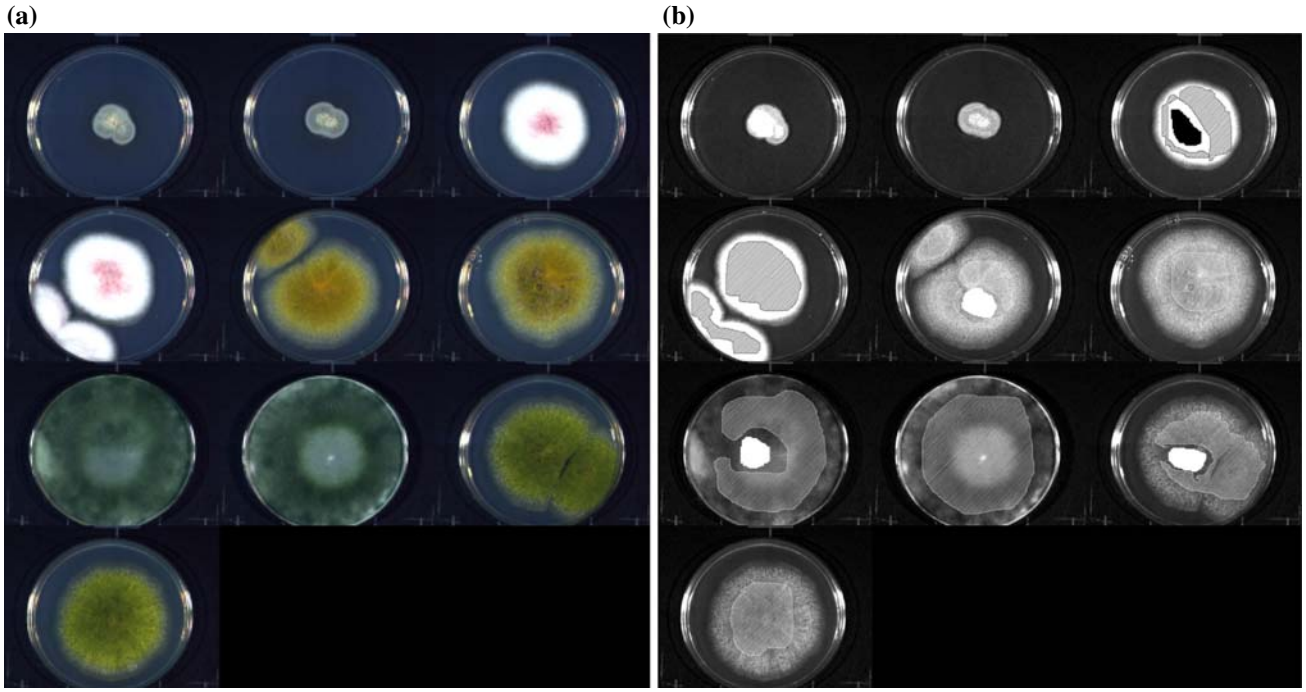

Penicillium chrysogenum	*Penicillium chrysogenum*	*Fusarium verticillioides*
Fusarium verticillioides	*Aspergillus parasiticus*	*Aspergillus parasiticus*
Trichoderma viride	*Trichoderma viride*	*Aspergillus flavus*
Aspergillus flavus	None	None

Fig. 3 (**a**) True color mosaic of the fungi used in experiment part A. (**b**) Regions of interest defined in experiment part A. The solid areas represent training regions and the line filled areas represent validation regions

The classification accuracy results are presented in a confusion matrix expressed in Table 5. Both *Fusarium* and *Penicillium* have high classification accuracy. The numbers are 99.2% and 99.9%, respectively. These numbers indicate *Fusarium* and *Penicillium* can be readily identified from the 5 candidate molds. The next highest accuracy is for *Trichoderma*, which is 98.6%. Error rate for the two *Aspergilli* are higher than the other three molds. The accuracy readings are 95.2% and 96.4% for *A. flavus* and *A. parasiticus*, respectively. The ML classifier is less precise in classifying the two *Aspergillus* species. About 4.6% of *A. flavus* was classified as *A. parasiticus.* Conversely,

Table 4 Results of SAS STEPWISE procedure for experiment part A with statistics of the first 10 selected bands

Step	Band	Wave-length (nm)	Partial *R*-square	*F*-Value	*P*-value	Wilks' Lambda	Pr <Lambda	Average squared canonical correlation
1	B121	743	0.9754	405843	<.0001	0.024603	<.0001	0.162566
2	B4	458	0.8855	79194.9	<.0001	0.002816	<.0001	0.310004
3	B38	541	0.6996	23839.6	<.0001	0.000846	<.0001	0.397645
4	B69	616	0.5942	14990.6	<.0001	0.000343	<.0001	0.466925
5	B171	864	0.3755	6153.92	<.0001	0.000214	<.0001	0.482929
6	B13	478	0.3348	5150.82	<.0001	0.000143	<.0001	0.493671
7	B91	670	0.2051	2640.96	<.0001	0.000113	<.0001	0.501568
8	B1	450	0.1564	1897.59	<.0001	9.56E-05	<.0001	0.508803
9	B25	509	0.157	1906.26	<.0001	8.06E-05	<.0001	0.515065
10	B51	572	0.1552	1881.04	<.0001	6.81E-05	<.0001	0.518388

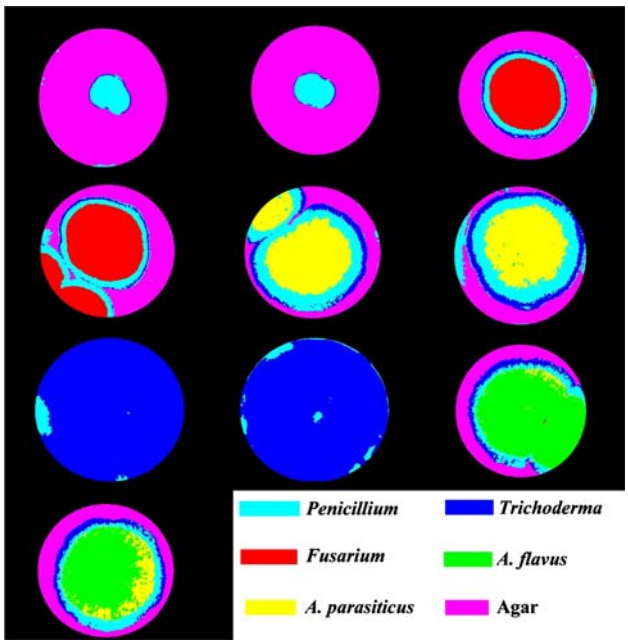

Fig. 4 Maximum Likelihood classification results for experiment part A. The classification used a reduced image space shown in Table 4

1.7% of *A. parasiticus* was classified as *A. flavus*. Another 1.7% of *A. parasiticus* was classified as *Penicillium*. The overall classification accuracy for experiment part A is 97.7%. One thing that the readers need to be aware of is that the validation data had to be selected manually, thus the results were to some extent subjective.

To further investigate the effect of image dimensionality over classification accuracy, the fungal image was classified using different image band combinations. Image bands used for this purpose were taken from the 10 most significant bands in Table 4, with a reduced order. For example, the top nine bands were used for classification, then the top eight bands, then seven, etc. The other reason for this study was practical application. For a conceptual fungal detection and identification device working in real-time situations, it would be desirable to use as few image bands as possible within acceptable detection accuracy. The resulting relationship curve between classification accuracy and image band number is plotted in Fig. 5. It is clear that when the number of bands used for classification dropped to two, classification accuracy reduced dramatically. Both the top three and top five band combinations have similar results, with the top five bands having the best overall accuracy. The top three bands are: band 121 (743 nm), band 4 (458 nm), and band 38 (541 nm), located in the near-infrared, middle of blue, and middle of green regions, respectively (Table 4).

Figure 6 is a plot of the five fungal signatures extracted from the classified image in experiment part A. Because each isolate was cultured in an individual dish and every effort was made to prevent cross contamination among the samples, the displayed fungal mean reflectance signature is assumed to be a pure signature. These signatures along with the calculated class statistics were used in experiment part B as training data for further classification of fungi.

It is obvious in Fig. 6 that the reflectance of *Fusarium* is markedly different from the other four isolates. This agrees with the previous observation in Fig. 3. *Trichoderma* and *Penicillium* have similar reflectance shapes, but different magnitudes. *A. flavus* and *A. parasiticus* reflectance is not

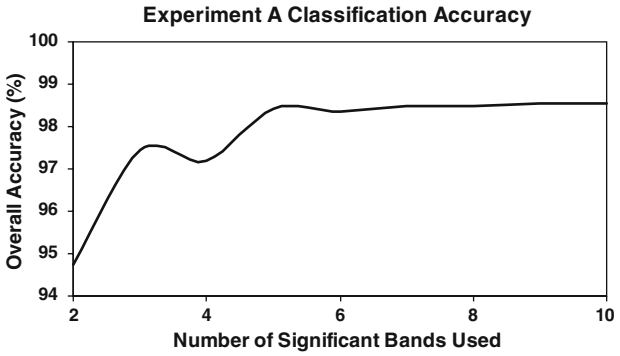

Fig. 5 Experiment part A: relationship between classification accuracy and the number of significant image bands used by the Maximum Likelihood classifier

Table 5 Confusion matrix used in assessing classification accuracy of experiment part A using the 10 most significant bands from Table 4

Class	Ground truth (Pixels)					Total
	Fusarium	*A. flavus*	*Trichoderma*	*A. parasiticus*	*Penicillium*	
Fusarium	78,638 (99.19%)	0 (0.00%)	0 (0.00%)	75 (0.12%)	0 (0.00%)	78,713
A. flavus	0 (0.00%)	86,752 (95.20%)	8 (0.00%)	1,094 (1.73%)	0 (0.00%)	87,854
Trichoderma	0 (0.00%)	40 (0.04%)	195,475 (98.61%)	0 (0.00%)	13 (0.12%)	195,528
A. parasiticus	0 (0.00%)	4,265 (4.68%)	0 (0.00%)	61,047 (96.41%)	0 (0.00%)	65,312
Penicillium	644 (0.81%)	73 (0.08%)	2,748 (1.39%)	1,106 (1.75%)	10,986 (99.88%)	15,557
Total ground truth pixels	79,282	91,130	198,231	63,322	10,999	442,964

The overall accuracy is 97.7276% (432,898/442,964) with the Kappa Coefficient equals 0.9679

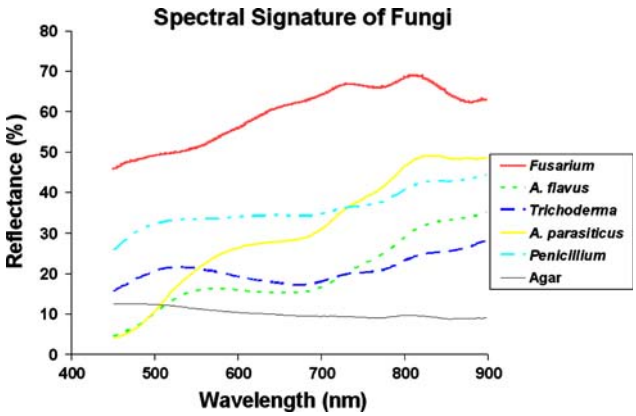

Fig. 6 Mold mean spectral curves

separable in the blue region, but starts to separate from the middle of the green region. Both *Aspergillus* species show stronger reflectance in the near infrared region than the visible light region, which is similar to reflectance measured over the canopy of a typical plant.

Experiment part B

Figure 7a depicts the true color image and Fig. 7b the regions of interest, of all fungal isolates in experiment part B. The name sequence can be found in Fig. 2 and Table 1. The growth pattern is similar to that in experiment part A. One phenomenon seen in part A is the rapid expansion of *Trichoderma*, which overtook the entire Petri dish during the culturing period. This same phenomenon can be seen in part B of the experiment. While the other four isolates all had moderate growth regions, *Trichoderma* spread out from the lower-right corner and "invaded" regions used by other isolates. One consequence is that the other four isolates might be contaminated by *Trichoderma*, which in turn will make fungal classification much more difficult in experiment part B compared to part A.

Figure 8 represents ML classification results for the samples in part B of the experiment. As in part A of the experiment, all the 'mature' fungi were classified. *Fusarium* and *Trichoderma* achieved a more accurate classification than the other three fungi. Although the pure *Penicillium*

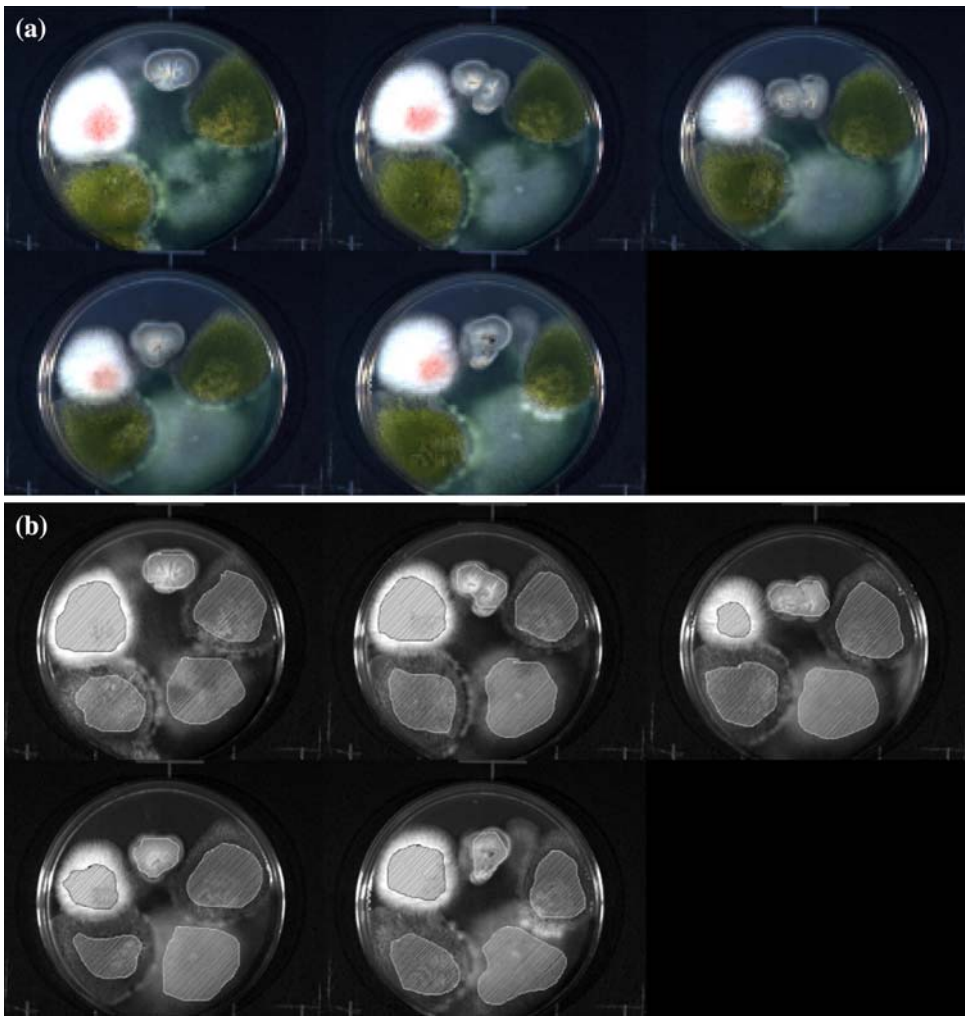

Fig. 7 (**a**) True color mosaic of the fungi used in experiment part B. (**b**) Regions of interest defined in experiment part B. The line filled areas represent validation regions. Classification training data was obtained from experiment part A

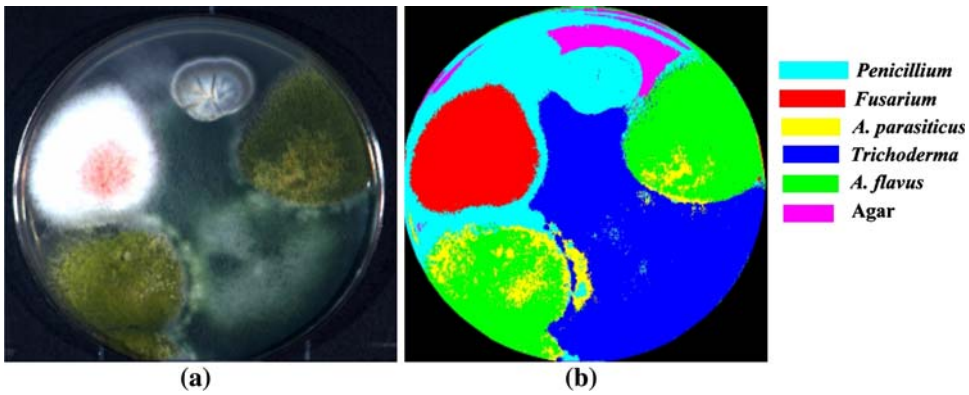

Fig. 8 Sample Maximum Likelihood classification results for experiment part B. The classification used a reduce image space as shown in Table 4

colony was correctly classified, a large portion of regions between *Penicillium* and *Fusarium*, and *Fusarium* and *A. parasiticus* were also mistakenly classified as *Penicillium*. *A. parasiticus* had the worst classification results. The classification accuracy results for experiment part B are presented in a confusion matrix expressed in Table 6. The overall classification accuracy value for experiment part B is 71.53%. For individual fungi, the accuracy is 99.6%, 97.1%, 70.6%, 8.3%, and 98.4% for *Fusarium, A. flavus*, *Trichoderma, A. parasiticus*, and *Penicillium*, respectively. The largest drop in classification accuracy was for *A. parasiticus*. A possible reason could be due to the contamination caused by *Trichoderma*, which was located next to *A. parasiticus*. Interestingly, contamination from *Trichoderma* did not have a strong influence over *A. flavus.* The observed effect was assumed to be due to difference in growth rates between the isolates. Classification accuracy for *Fusarium* and *Penicillium* remained equivalent to results in part A of the experiment.

Similar to experiment part A, the relationship between classification accuracy and image band number was also studied and the results are plotted in Fig. 9. The overall classification accuracy dropped steadily from nine bands to four bands. The peak accuracy appeared when only the top three most significant bands were used (Table 4). Combined results from both parts of the experiment A and B

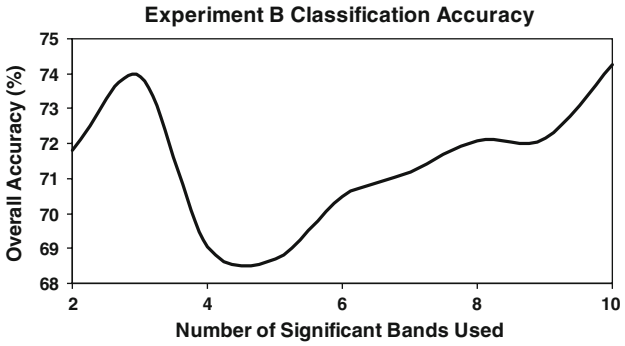

Fig. 9 Experiment part B: Relationship between classification accuracy and the number of significant image bands used by the Maximum Likelihood classifier

suggest using three image bands for classification of the five, above mentioned, toxigenic fungi.

Conclusions

The current project studied reflectance of five fungi including *Fusarium*, *A. flavus*, *Trichoderma, A. parasiticus*, and *Penicillium* using visible near infrared hyperspectral imagery collected with a pushbroom image sensor. The study consisted of two parts, A and B. In experiment part A, each fungus was cultured in individual Petri dishes. In

Table 6 Confusion matrix used in assessing classification accuracy of experiment part B using the 10 most significant bands in Table 4

Class	Ground truth (Pixels)					Total
	Fusarium	*A. flavus*	*Trichoderma*	*A. parasiticus*	*Penicillium*	
Fusarium	54,648 (99.66%)	0 (0.00%)	0 (0.00%)	1 (0.00%)	59 (0.20%)	54,708
A. flavus	0 (0.00%)	70,801 (97.16%)	61 (0.06%)	59,955 (91.69%)	48 (0.16%)	130,865
Trichoderma	0 (0.00%)	139 (0.19%)	67,745 (70.65%)	1 (0.00%)	346 (1.15%)	68,231
A. parasiticus	0 (0.00%)	1,921 (2.64%)	621 (0.65%)	5,420 (8.29%)	23 (0.08%)	7,985
Penicillium	187 (0.34%)	7 (0.01%)	27,461 (28.64%)	10 (0.02%)	29,571 (98.42%)	57,236
Total ground truth pixels	54,835	72,868	95,888	65,387	30,047	319,025

The overall accuracy is 71.53%, with the Kappa Coefficient equals 0.6398

experiment part B, all five species were cultured in a single dish. Images were classified in a reduced image space with 10 bands selected from the original images. The overall fungal classification accuracy in experiment part A was 97.7% while in experiment part B the accuracy dropped to 71.5%. A possible reason could be that the rapid growth of *Trichoderma* in experiment part B contaminated spectral reflectance features of the other four isolates. Separability analysis of the pure fungal signatures in part A of the experiment indicates the five fungi are separable to a high degree of accuracy. It was concluded from both parts of the experiment that by using three narrow bands (bandwidth = 2.43 nm) centered at 743 nm, 458 nm, and 541 nm, the five fungal species studied in the present paper could be well separated. Additionally, the experiment demonstrated the feasibility of the application of hyperspectral imaging in mold identification.

Acknowledgements This research was carried out in accordance with the USDA Specific Cooperative Agreement No. 58-6435-3-0121. Funding for the current project was provided through the USDA Specific Cooperative Agreement No. 58-6435-3-0121. The authors gratefully acknowledge the expert assistance of Mr. David Ambrogio and Ms. Ahline Angeles with specimen preparation, and Mr. Kevin DiCrispino with data processing.

References

1. C.P. Wild, P.C. Turner, Mutagenesis **17**, 471 (2002)
2. H.P. van Egmond, M.A. Jonker, Worldwide regulations for mycotoxins in food and feed in 2003. *Published by FAO as Food and Nutrition Paper No. 81* (2005)
3. R.L. Brown et al., J. Food Prot. **64**, 396 (2001)
4. E. Collison et al., J. Hyg. Epidemiol. Microbiol. Immunol. **36**, 338 (1992)
5. J. Duvick, Environ. Health Perspect. **109**, 337 (2001)
6. A.E. Desjardins, G. Manandhar et al., Appl. Environ. Microbiol. **66**, 1020 (2000)
7. P.E. Nelson et al., Clin. Microbiol. Rev. **7**, 479 (1994)
8. N.H. Aziz, A.A.M. Shahin, J. Food Prod. **17**, 113 (1997)
9. B.R. Malone et al., J. AOAC Int. **83**, 95 (2000)
10. H.J. Zeringue Jr. et al., Phytochemistry **52**, 1391 (1999)
11. I. Zachova et al., Folia Microbiol. **48**, 817 (2003)
12. T.K. Dutta, P. Das, Mycopathologia **151**, 29 (2001)
13. J. Jaimez Ordaz et al., Int. J. Food Microbiol. **83**, 219 (2003)
14. C.A. Fente et al., Applied Environ. Microbiol. **67,** 4858 (2001)
15. G.S. Birth, R.M. Johnson, J. Assoc. Off. Anal. Chem. **53**, 931 (1970)
16. K. Yabe et al., Appl. Environ. Microbiol. **53**, 230 (1987)
17. D.T. Wicklow, Plant Dis. **83**, 1146 (1999)
18. J. Aja-Nwachukwu, S.O. Emejuaiwe, Environ. Toxicol. Water Qual. An. Int. J. **9**, 17 (1997)
19. S.H. Gordon et al., Int. J. Food Microbiol. **35**, 179 (1997)
20. S.H. Gordon et al., J. Food Prot. **61**, 221 (1998)
21. S.H. Gordon et al., J. Agric. Food. Chem. **47**, 5267 (1999)
22. R.V. Greene et al., J. Agric. Food Chem. **40**, 1144 (1992)
23. P. Yu, J. Struct. Biol. **150**, 81 (2005)
24. M.S. Kim et al., Trans. ASAE **44**, 721 (2001)
25. R. Lu, Trans. ASAE **46**, 523 (2003)
26. K.C. Lawrence et al., ASAE Paper No. 013129 (2001)
27. B. Park et al., Trans. ASAE **45**, 2017 (2002)
28. I. Kim et al., Trans. ASAE **47**, 1785 (2004)
29. B.A. Weinstock, Appl. Spectroc. **60**, 9 (2006)
30. H. Yao et al., in *Proceedings of SPIE, Optic East, a SPIE Conference on Nondestructive Sensing for Food Safety, Quality, and Natural Resources* (2004)
31. C. Mao, U.S. patent 6,166,373 (2000)
32. E.N. VI, *ENVI Users Manual* (Research Systems Inc, Boulder, CO, 2000)
33. G.F. Hughes, Trans. IEEE **14**, 55 (1968)
34. SAS Users Manual, SAS Institute, Inc.Cary, NC (2003)